Microstructural, Thermal, Crystallization, and Water Absorption Properties of Films Prepared from Never-Dried and Freeze-Dried Cellulose Nanocrystals

Kazi M. Zakir Hossain,* Vincenzo Calabrese, Marcelo A. da Silva, Julien Schmitt, Saffron J. Bryant, Md Towhidul Islam, Reda M. Felfel, Janet L. Scott, and Karen J. Edler

In this paper, the microstructural, optical, thermal, crystallization, and water absorption properties of films prepared from never-dried (ND) and freeze-dried (FD) cellulose nanocrystals (CNCs) are reported. Morphology of the ND CNCs reveals a needle-like structure, while after freeze-drying, they show a flake-like morphology. Microstructural analysis of ND and FD CNCs are further studied via small angle X-ray scattering to probe interactions. ND CNCs yield a transparent film with a low surface roughness (14 ± 4 nm), while the FD CNC film evidence a significant reduction of their transparency due to their higher surface roughness (134 ± 20 nm). Although Fourier transform infrared spectroscopy and energy-dispersive X-ray spectroscopy analyses reveal no chemical change occurs during the freeze-drying process, yet a more intense thermal degradation profile is observed for FD CNC film, probably due to the higher oxygen ingress within the gaps created between the stacked flakes. This, in turn, results in a greater loss of crystallinity at a higher temperature (300 °C) compared to the ND CNC film. A rapid decrease in water contact angle of the FD CNC film proves that the morphology of flakes and their orientation within the film has a strong influence in increasing water absorption capacity.

1. Introduction

The demand for the utilization of bio-derived and biodegradable materials, such as cellulose, in diverse fields, including food, cosmetic, pharmaceuticals, green packaging, electronics, barrier films, nanocomposites, membranes, and super capacitors[1,2] is growing significantly to ensure a sustainable future. Cellulose is the most abundant natural polymer and can be treated into various forms, such as nanofibrils and nanocrystals.[2] Their nanoscale dimensions, high elastic modulus, as well as the presence of highly reactive surfaces, makes them a promising reinforcing nanomaterial.[3] The nanocellulose materials have also been extensively investigated with diverse cell lines and assay revealing no (or relatively very low) cytotoxicity.[4–6] Additionally, their excellent bioconjugation properties suggested the possibilities of the use of nanocellulose-based materials in various therapeutic applications, including targeting and the controlled release of drugs.[7–9]

Nanocelluloses are generally processed either via chemical treatment (such as acid hydrolysis process) or mechanical methods using high-pressure homogenizer or grinder.[10–12] In the acid hydrolysis process, hydrolysis of amorphous regions of cellulose fibrils using a suitable concentration of acid takes place, leaving the crystalline area in the form of cellulose nanocrystals (CNCs).[13,14] The mechanical

Dr. K. M. Z. Hossain, Dr. V. Calabrese, Dr. M. A. da Silva, Dr. J. Schmitt,[+]
Dr. S. J. Bryant, Prof. J. L. Scott, Prof. K. J. Edler
Department of Chemistry
University of Bath
Claverton Down, Bath BA2 7AY, UK
E-mail: z.hossain@bath.ac.uk

[+]Present address: LSFC – Laboratoire de Synthèse et Fonctionnalisation des Céramiques, UMR 3080 CNRS / Saint-Gobain CREE, Saint-Gobain Research Provence, 550 avenue Alphonse Jauffret, Cavaillon, France

Dr. M. T. Islam
Department of Applied Chemistry and Chemical Engineering
Faculty of Engineering
Noakhali Science and Technology University
Noakhali 3814, Bangladesh

Dr. M. T. Islam, Dr. R. M. Felfel
Advanced Materials Research Group
Faculty of Engineering
University of Nottingham
Nottingham NG7 2RD, UK

Dr. R. M. Felfel
Physics Department
Faculty of Science
Mansoura University
Mansoura 35516, Egypt

Prof. J. L. Scott, Prof. K. J. Edler
Centre for Sustainable Chemical Technologies
University of Bath
Claverton Down, Bath BA2 7AY, UK

treatment instead involves physical defibrillation of the cellulose microfibrils to produce cellulose nanofibrils (CNFs) with a typical dimension of 3–5 nm in diameter and several microns in length.[15,16] However, high energy consumption associated with the mechanical process is a drawback for CNF production unless a chemical pre-treatment on the source cellulose is performed.[10,17]

CNCs are widely produced from cotton,[18] wood pulp,[19] tunicate,[20] sisal,[21] and ramie[22] using sulfuric or hydrochloric acid hydrolysis process. The diameter and length of CNCs vary depending on the source of the cellulose and process parameters (type and concentration of acid, hydrolysis time, and temperature).[3,20,23,24] For example, CNCs extracted from cotton via acid hydrolysis process are reported to be 5 to 15 nm in width and 50 to 300 nm long, while the CNCs isolated from tunicates are typically 10–30 nm in width and 100–4000 nm long.[11,20,25]

CNCs showed good stable dispersion in aqueous solution due to their tunable surface charge, especially in their never-dried state. Commonly, the term "never-dried" used in nanocellulose research to describe the as received aqueous dispersion of cellulose nanocrystals or nanofibrils obtained after processing from their various sources, which never undergoes any dehydration process. Never-dried CNCs in their aqueous suspension can maintain their individual shape by preventing aggregation when an appropriate surface charge is incorporated; however, they tend to agglomerate during either air, oven, or freeze-drying processes because of their intermolecular hydrogen bonding.[26,27]

Despite the aggregation, drying of CNCs is arguably required when considering blending with water-insoluble hydrophobic polymers in nanocomposite fabrication[28] as well as for long-term preservation.[29] On the other hand, upon drying, strong inter-particle hydrogen bonds are usually formed in the self-assembled dried CNCs, which are very difficult to break, making them hard to redisperse if they do not possess enough surface charge to impart the required repulsion forces in solution.[30] In addition, high energy sonication is essential for this re-dispersion process, which can be an economic limitation when handling a large amount of freeze-dried particles for industrial applications.[31]

To expand the applications, different microstructures, as well as geometries, can be achieved by employing different drying conditions.[32] For example, never-dried CNC suspended in water are dispersed as needle-like particles,[33] whereas a spherical shape was obtained by spray drying, and freeze-drying yielded larger flakes and foam-like structures.[32] Self-assembling behavior of CNCs during drying has been reported to be remarkably influenced by the suspension concentration, surface charge and crystal structure, as investigated by Han et al.[34] They suggested that lamellar structured flakes were formed upon freeze-drying of 0.5 to 1 wt% suspension via alignment of CNCs along the direction of growth of ice crystals.

The freeze-drying technique has also been investigated in producing cellulose foams with different microstructures.[34,35] Cellulose microfibril foams with a lamellar structure were investigated by Lee and Deng[36] using a directional freezing technique.

The distinctive morphology obtained from ND CNCs and FD CNCs can be utilized to produce films with various surface textures to control optical transparency, and their ability to influence the moisture barrier as well as absorption properties. In this study, self-assembled cellulose film was prepared from a stable aqueous dispersion of ND CNCs using the air-drying process at room temperature. For comparison, another pure cellulose film was prepared from the FD CNCs (which were also produced from the same ND CNC suspension after quick freezing using liquid nitrogen followed by freeze-drying) via casting from their aqueous suspension. The influence of the microstructures created during the air and freeze-drying processes on morphological, surface roughness, light transparency, nanoscale structure (measured by small angle X-ray scattering (SAXS)), ζ-potential, thermal, crystallization, and water contact angle properties were investigated. Although several studies on the aggregation behavior of cellulose nanocrystals during varying drying conditions have been reported,[34–38] this study, however, aimed to conduct a comparative study on the film properties prepared from same nanocrystals but employing two different drying processes. It is expected that a detailed understanding of properties mentioned above influenced by their microstructures will provide fundamental guidance for the development of sustainable cellulose-based films for diverse applications, including packaging, barrier films, electronics and biosensors.

2. Results and Discussion

Never-dried CNCs were prepared via sulfuric acid hydrolysis of cotton wool; followed by freezing in liquid nitrogen and freeze-drying to obtain freeze-dried CNCs, as shown in **Figure 1**a–c. The ND CNC suspension (1.15 wt% in DI water) was observed to be stable as no precipitation was seen after long time storage (≈6 months), as can be seen in Figure 1b. In contrast, the CNCs obtained after the freeze-drying process were white and fluffy, presenting a foam-like structure (Figure 1c). The microstructure of these cellulose particles was characterized via electron microscopy. Fibrillar morphology of the cotton wool prior to acid hydrolysis was observed (see Figure 1d), while after acid hydrolysis the ND CNC exhibited needle-like particles (TEM micrograph in Figure 1e) with average length ≈140 ± 50 nm and width (at major radius) 20 ± 5 nm. The freeze-dried CNCs exhibited flake-like morphology along with some fibrillar shaped particles in micron-range size, as can be seen in Figure 1f.

It is well known that some factors, like particle size and concentration as well as surface charge or method of freezing, are crucial in controlling the morphology of particles during the freeze-drying process.[35,39] In the freezing cycle, the CNCs are confined into interstitial spaces between the ice crystals and during the drying process, irregular shaped flake-like structures are formed, as illustrated in **Figure 2**. Han et al. suggested that the CNCs were initially self-assembled longitudinally to form micron-sized cellulose fibers that were further self-organized in parallel to form flake-like structures during the freeze-drying process.[34] They also reported that the reduction of the CNC suspension concentration from 1.0 to 0.05 wt% before freeze-drying could result in the formation of ultra-fine cellulose fibers rather than the flake by minimizing their parallel self-assembly. Thus, the combination of micron-sized flakes and ribbon-like fibers obtained in this study after freeze-drying
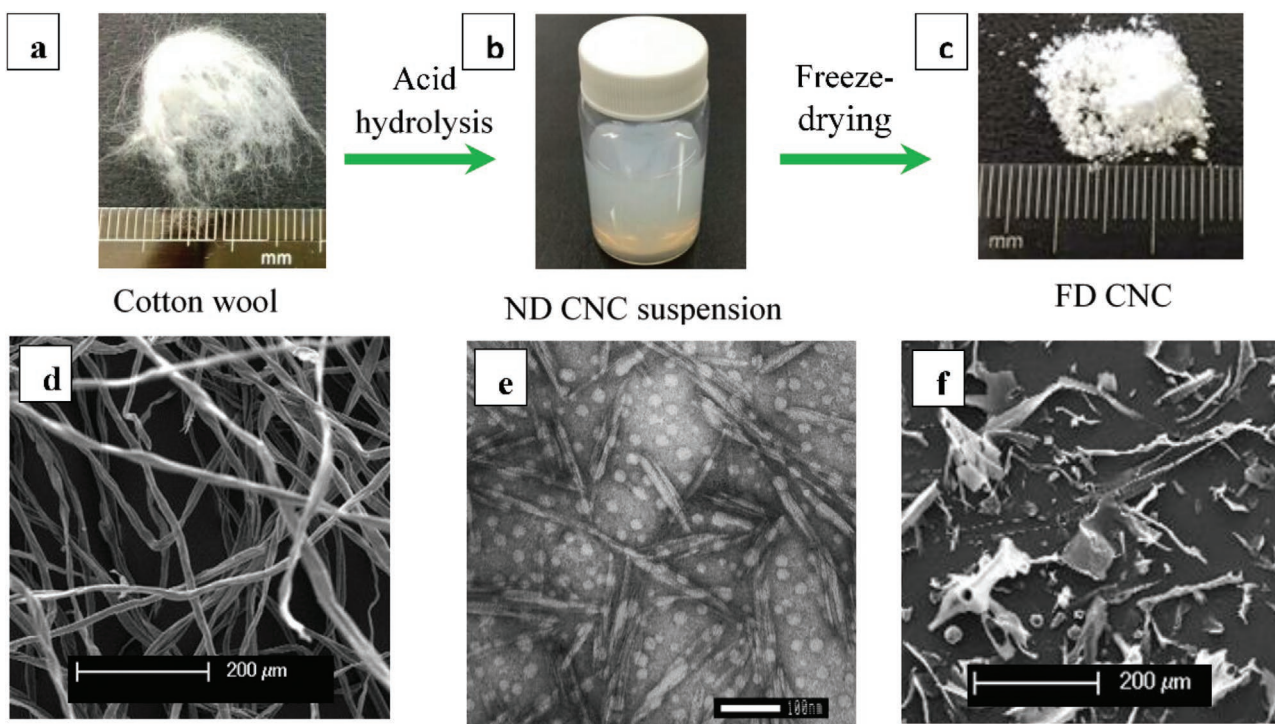
Figure 1. a) Photographs show the cotton wool, b) ND CNC suspension (1.15 wt% in DI water) obtained after sulfuric acid hydrolysis process, c) FD CNCs obtained after freeze-drying, d) SEM micrograph of the cotton wool, e) TEM micrograph of ND CNCs (uranyl acetate solution was used here as a contrasting agent, scale bar 100 nm), and f) SEM micrograph of FD CNCs.

of CNC demonstrates the formation of self-assembled CNCs along with their longitudinal and parallel directions.

The microstructural characterization of the ND and FD CNC suspensions were also investigated via SAXS. The change in morphology is evident from the SAXS patterns (**Figure 3**). Indeed, the SAXS data obtained for ND CNCs in water were fitted using a rigid elliptical cylinder model with a fixed length of 140 nm (derived from TEM measurements) and minor and major radius of 2.5 and 25 nm, respectively (see Figure 3a for the data and fit, and **Table 1** for the fitting parameters), which is in good agreement with their needle-like shape as evidenced by the TEM image. At low-q, ND CNCs (0.1 wt%) showed the char-

acteristic q^{-1} slope associated with non-interacting elongated objects; consistent with CNC at that concentration.[40] Moreover, the SAXS patterns of the ND CNC suspension revealed that their intensity increases with the suspension concentration (Figure 3a), which is expected as $I(q)$ is proportional to the number of objects in the suspension.

In contrast, the scattering pattern observed for FD CNCs resuspended in water (Figure 3b) strongly diverged compared to the signal of ND CNCs. It is explained earlier that the FD CNCs formed into the micron-sized flake-like object via self-assembly during the freeze-drying process. To resuspend these FD CNCs in DI water, a comparatively aggressive redispersion
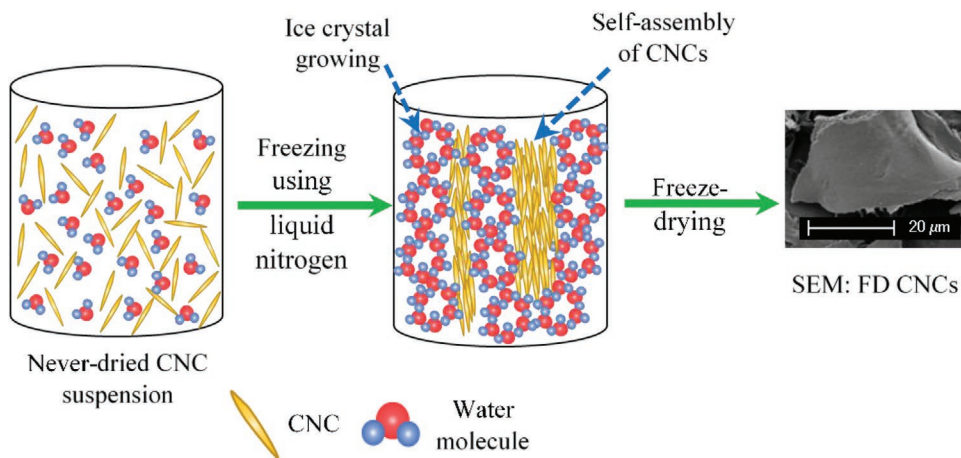

Figure 2. Representative illustration shows the formation of flake-like CNC particles during the freeze-drying process. Illustration not drawn to scale.

**ADVANCED
SCIENCE NEWS**

www.advancedsciencenews.com

**Macromolecular
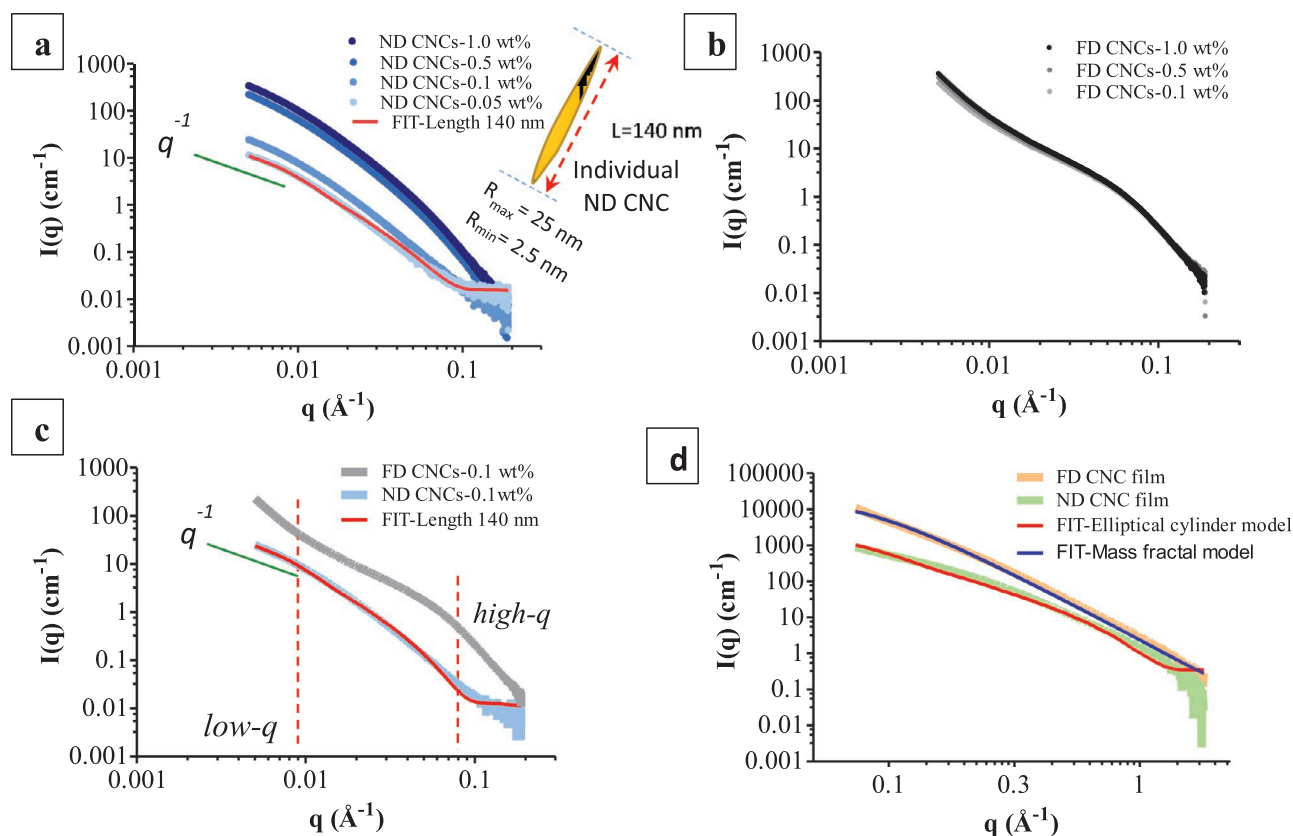Materials and Engineering**

www.mme-journal.de

Figure 3. Small-angle x-ray scattering (SAXS) patterns of a) ND CNCs and b) FD CNC suspensions at various concentrations (values in the illustration are used from the SAXS fitting parameters). c) Comparison of SAXS curves of ND and FD CNC suspensions at a fixed concentration of 0.1 wt% and d) SAXS curves of the films produced from ND and FD CNCs.

process was employed, where the sonication probe was used at higher amplitude (30%) for a more extended period (10 min), as mentioned in the Experimental Section. However, due to the lack of enough surface charge (ζ-potential <−30 mV), it was hard to redisperse the dried flake-like particles into individual needle-shaped CNCs. Liu et al. also suggested that the cohesion force of sulfated CNC film was too strong to redisperse in the aqueous medium due to their intermolecular hydrogen bonding.[38] In addition, sedimentation within the capillary for the FD CNC suspension was observed (see Figure S2 in the Supporting Information). Therefore, the SAXS pattern obtained for the FD CNCs (Figure 3c) may be a representation of the comparatively smaller size range FD CNC particles, which were still suspended within the probe area of the capillary even after sedimentation of the larger flake-like particles. Thus, the FD CNCs showed very little increase in their scattering intensity with increasing concentration in the probed q-range, as can be

seen in Figure 3b. Therefore, in this case, due to their various sizes, the SAXS fitting would not be truly representative for the actual FD CNC microstructure obtained after freeze-drying (thus, fitting was avoided for the FD CNC suspension).

SAXS analysis of ND and FD CNC films was also performed on an Anton-Paar SAXSpoint 2.0 covering the q range of about 0.07–1.8 Å^{-1}. The scattering data from the ND CNC film was also fitted using a rigid elliptical cylinder model considering the same fitting parameters (except for the scaling factor, see Table 1) used for the scattering of ND CNC suspension. This suggests that the individual CNC particles remained as discrete scattering objects on the SAXS length scale even after drying into a film, which is also evidenced by the 2D AFM image of the ND CNC film, shown later in **Figure 4**d. On the other hand, we were unable to fit the scattering intensity of the FD CNC film using the same elliptical cylinder model. This might be due to the formation of flake-like micron sized CNC particles

Table 1. Parameters obtained by fitting of the SAXS data for ND CNC suspension and films produced from ND and FD CNCs.

	Model[b]	Radius-minor [nm]	Radius-major [nm]	Length [nm]	Fractal dimension
ND CNC suspension[a]	Rigid elliptical cylinder	2.5 ± 0.1	25	140	–
ND CNC film	Rigid elliptical cylinder	2.5	25	140	–
FD CNC film	Mass fractal	–	–	–	2.9

[a]SAXS data for 0.1 wt% ND CNC suspension; [b]SLD (scattering length density) for cellulose and solvent: 13.5×10^{-6} and 9.5×10^{-6} Å^{-2}, respectively.

**ADVANCED
SCIENCE NEWS**
www.advancedsciencenews.com

**Macromolecular
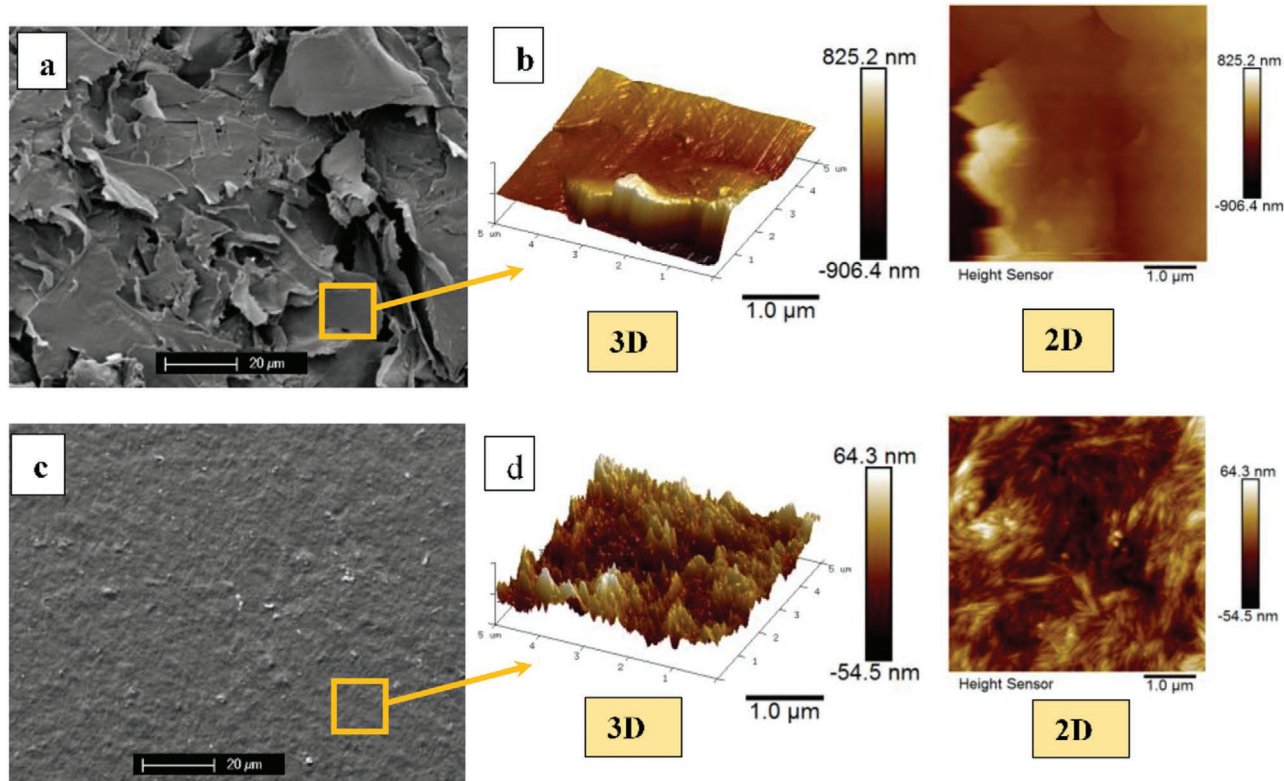Materials and Engineering**
www.mme-journal.de

Figure 4. a) SEM micrograph of freeze-dried (FD) CNC film, b) AFM images (2D and 3D) of FD CNCs film, c) SEM micrograph of never-dried (ND) CNC film, and d) AFM images (2D and 3D) of ND CNCs film.

during the freeze-drying process, in which no individual needle-like fibrils were observed, as can be seen by SEM and AFM images in Figure 4a,b. However, the scattering pattern of FD CNC film can be fitted using mass fractal model (shape independent) with fractal dimension (d_f) around 2.9, indicating the internal film structure is fractal.[41] The fractal dimension is directly associated with the compactness of the aggregated CNCs, as suggested by Phan-Xuan et al., who also investigated the aggregation behavior of CNCs in the presence of various salt concentrations.[37]

Cellulose particles prepared in this study had negatively charged surfaces due to the presence of sulfate group on the CNC surface. The ζ-potential values of ND CNCs and FD CNCs after re-dispersion were found to be −23 ± 2 and −18 ± 3 mV, respectively. This suggests no significant change in surface charge of the dispersed particles due to the freeze-drying process, although sedimented flakes could not be measured. Particles having a ζ-potential between ±30 mV have been suggested to possess weak mutual electrostatic repulsion forces;[34] as a consequence, the ND CNCs produced in this study were easier to self-assemble into flakes after freeze-drying due to their lower zeta potential.

We prepared films using both FD CNCs and ND CNCs, via a solution casting process. Both films were characterized via SEM and AFM for their surface topography and roughness analysis. From SEM and AFM data, FD CNC film consists in the deposition of the FD-CNC flakes in a random pattern resulting in a rough and porous film, as can be seen in Figure 4a. Both

3D and 2D (height sensor) AFM images, focusing on an area of 5 μm × 5 μm, also show the flake-like morphology in the film (Figure 4b), while no individual needle-like fibrils can be observed. The surface roughness, R_a, of the FD CNC film was found to be 134 ± 20 nm. This value represents the average surface roughness of an individual flake, not the entire film, as the dimension of the flakes was seen to be higher than the measured area (see the SEM micrograph in Figure 4a). By comparison, the ND CNC film surface revealed the uniform distribution of the particles, with low surface roughness and no porosity (see Figure 4c). From the 3D AFM image analysis, the surface roughness was found at 14 ± 4 nm. Here, the film results from the dense packing of ND CNC in chiral nematic (cholesteric) organizations,[42] as it can be observed in the 2D (height) AFM image (see Figure 4d).

The structural differences of the films affect their macroscopic properties, with the ND CNC film being transparent, while the FD CNC film is white, paper-like and opaque (**Figure 5**a). Quantitatively, UV/Visible spectrometry also showed that the ND CNC film exhibited light transmittance of ≈90% in most of the visible light region, whereas, the FD CNC film exhibited less than 1% light transmittance (Figure 5b). It is well known that the roughness of the surface of the nanocellulose film significantly reduces the light transmittance due to light scattering effects.[43] Thus, the higher surface roughness of the FD CNC film due to the random orientation of the micron-sized flakes, as discussed earlier, is responsible for its poor optical properties. Alternatively, the higher light transparency of the ND CNC film
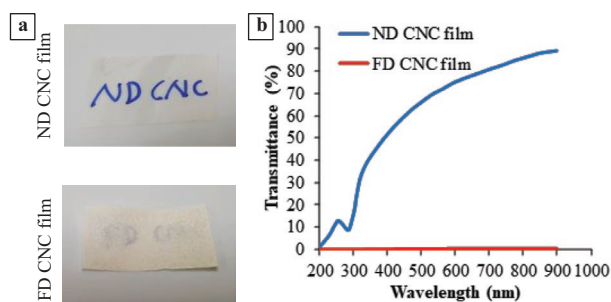
Figure 5. a) Representative photographs of the transparent ND CNC film (top) and paper-like opaque FD CNC (bottom) film, and b) light transmittance of thin films obtained by UV/Visible spectrometry.

obtained in this study was due to their well-dispersed needle-like structure prior to the film formation and hence a comparatively lower surface roughness (≈14 ± 4 nm) and denser packing of the needle-like CNCs in the film. Also, the ND CNC film prepared in this study was very much looked like thin transparent glass. However, due to the lower aspect ratio and high mechanical

properties of the individual CNC particle (elastic modulus of the cotton-based CNCs was reported to be 57 to 105 GPa along the axial direction),[44] the film produced from the ND CNCs was too brittle to cut into a strip for tensile testing. Therefore, mechanical properties were not assessed for these films.

The principal chemical groups of the ND CNC and FD CNC films were identified using FTIR-ATR analysis as presented in **Figure 6**a. Both films showed a similarly broad spectrum peak at 3335 cm^{-1} that was attributed to a free –OH stretching vibration. The bands at 2900 and 1427 cm^{-1} indicate the C–H stretching vibration. The peak at 1160 cm^{-1} was attributed to the C–O–C stretching bridge of the glucose ring structure of cellulose. The bands at 1053 and 1030 cm^{-1} represents the C–O stretching at position C-6 and C-3 in the saccharide structure, respectively.[45] The bands at 896 cm^{-1} were attributed to the β-glycosidic linkage in cellulose.[46] The absorbance band at 807 cm^{-1} representing the C–O–S vibration associated with the C-O-SO$_3$ group present on the surface of the CNCs was expected,[34] due to the esterification of hydroxyl groups by sulfate ions formed during the sulfuric acid hydrolysis process employed to extract the CNC from cotton. In the case of both films, no new bands were detected as well as no noticeable
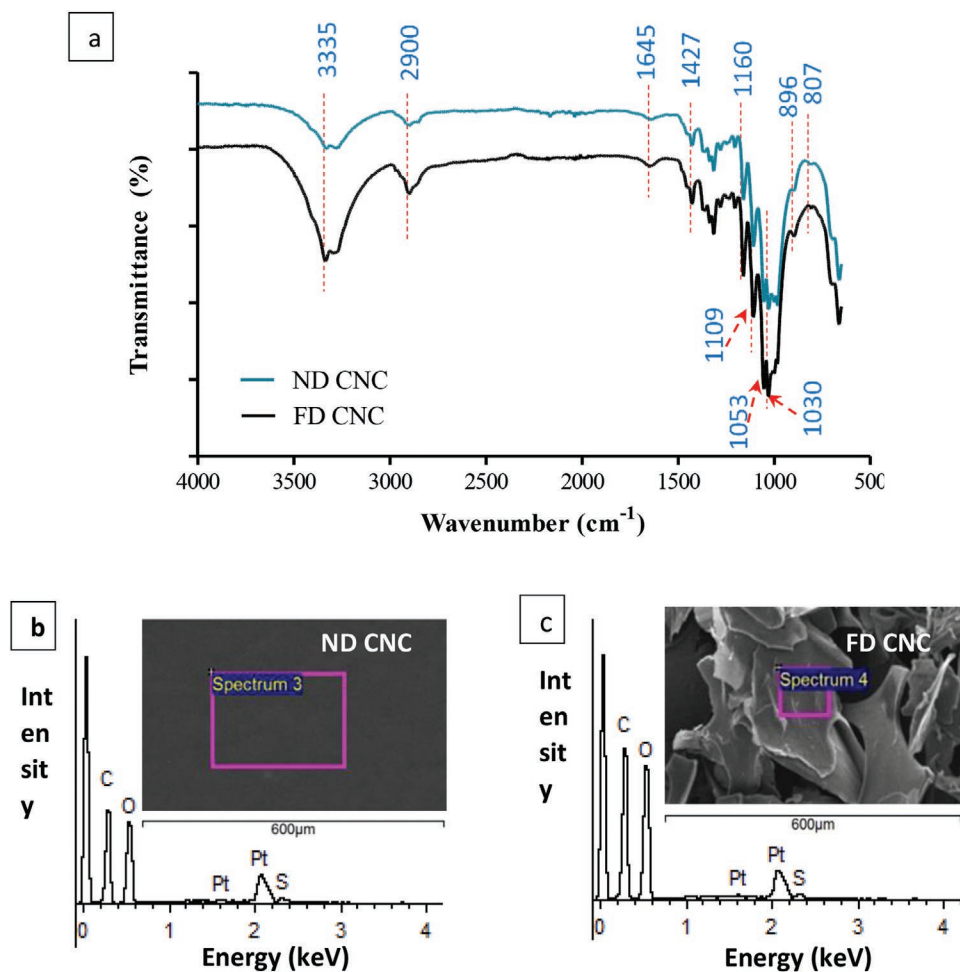

Figure 6. a) FTIR spectroscopy spectra of never-dried and freeze-dried CNC films. b,c) Energy-dispersive X-ray spectroscopy (EDX) spectra of ND and FD CNC films (insets show the SEM images highlighting the areas scanned for compositional analysis).

**ADVANCED
SCIENCE NEWS**

www.advancedsciencenews.com

**Macromolecular
Materials and Engineering**

www.mme-journal.de

Table 2. Chemical compositions of ND CNC and FD CNC films determined using EDX.

Films	Element					
	C		O		S	
	weight%	atomic%	weight%	atomic%	weight%	atomic%
ND CNC	48.40	55.72	50.97	44.01	0.63	0.27
FD CNC	48.21	55.50	51.27	44.27	0.52	0.23

band shift was observed, which indicated that there was no chemical change after freeze-drying.

The chemical compositions of the ND and FD CNC films were also characterized using an energy-dispersive X-ray spectroscopy (EDX) detector attached to the SEM. Figure 6b,c shows the EDX spectra of the ND and FD CNC films. The peaks around 0.3, 0.5, and 2.3 keV were associated with the binding energies of carbon, oxygen and sulfur, respectively, which is found consistent with the literature.[47,48] The weight and atomic percentages of chemical elements of both films are summarized in **Table 2**. The ND CNC film contains 0.63 wt% elemental sulfur (due to sulfuric acid hydrolysis process) along with the main components such as carbon (48.40%), and oxygen (50.97%), which matches well with the values of CNCs suggested by Man et al. (C = 47.69, O = 51.63, and S = 0.68 wt%).[47] As expected, no remarkable compositional changes in the film was observed after freeze-drying the CNCs.

Thermogravimetry (TG) and derivative thermogravimetry (DTG) curves of the ND CNC and FD CNC films are shown in **Figure 7**. From the derivative thermogravimetry (DTG) curves, the onset temperature of initial thermal decomposition ($T_{d\ (initial)}$) of both CNC films was observed at 132 °C with maximum decomposition temperature for the initial combustion reaction ($T_{max(initial)}$) at 166 °C (FD CNC) and 174 °C (ND CNC) (see Figure 7b), where the loss of low molecular mass fragments was suggested.[49]

In addition, TGA curves revealed that the mass loss of FD CNC film during the initial thermal decomposition reaction was not as pronounced as the ND CNC film (also evidenced from the initial thermal decomposition peaks from the DTG curves). This suggests that the diffusion of heat is slower in the case of FD CNC film due to their greater thickness (80 ± 5 µm), which is expected, compared to the ND CNC film (50 ± 5 µm thick). In addition, the larger sized flakes within the FD film may be more stable, protecting some of the central portions of the film at lower thermal degradation temperatures. Thus, the weight loss of FD CNC and ND CNC films at the initial degradation temperature ($T_{max(initial)}$) was found to be around 4.5% and 8.2%, respectively. FD CNC and ND CNC films showed the onset temperature of the major combustion reaction ($T_{d\ (major)}$) at 186 and 196 °C, respectively, pinpointing the commencement of the thermal degradation of all the major chemical groups of cellulose through solid-state transformations.[49,50] The maximum decomposition temperatures ($T_{max(major)}$) for ND CNC film is found at 307 °C (from the DTG curves). While a more intense major combustion reaction can be observed in the case of the FD CNC film with a peak maximum at 287 °C. This may be due to the higher amount of oxygen ingress in the gaps created in between the randomly stacked FD CNC flakes (as evidenced from the SEM image in Figure 4a), which was

suggested to be favorable for the major combustion reaction.[51] Two additional peaks obtained at 240 and 315 °C might be associated with the thermal degradation of comparatively lower and higher mass fragments (respectively) of the major chemical groups in the crystalline region. Pan and Richards [52] reported that the thermal degradation of cellulose by heating above 250 °C was due to dehydration from the crystalline area of cellulose by elimination reactions from the hydroxyl groups to yield unsaturated systems and ultimately char (investigated using TG-FTIR). Julien et al. [53] also reported that the thermal decomposition of cellulose at a temperature from 210 to 325 °C was due to dehydration reactions, as observed by a decrease in the intensities of IR absorption bands at 3300–3400 cm⁻¹ associated with the hydroxyl group stretching. After the major combustion reaction (400 °C), the residual char weight of ND CNC and FD CNC films was 36% and 29%, respectively.

A summary of the thermogravimetry analysis (TGA and DTG) data are presented in **Table 3** and represents the
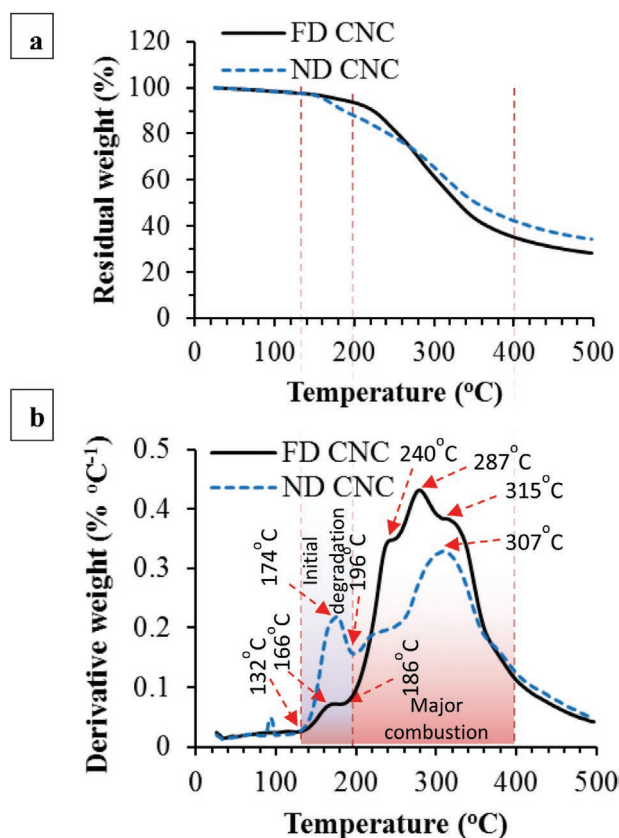
Figure 7. a) TGA and b) DTG curves of never-dried and freeze-dried CNC films.

**ADVANCED
SCIENCE NEWS**
www.advancedsciencenews.com

**Macromolecular
Materials and Engineering**
www.mme-journal.de

Table 3. Summary of TGA data obtained for ND CNC and FD CNC films.

Films	Initial thermal degradation profile			Major thermal decomposition profile		
	$T_{d\ (initial)}$ [°C] (from DTG curves)	$T_{max\ (initial)}$ [°C] (from DTG curves)	Weight loss at $T_{max\ (initial)}$ [%] (from TGA curves)	$T_{d\ (major)}$ [°C] (from DTG curves)	T_{max} [°C] (from DTG curves)	Weight loss at $T_{max\ (major)}$ [%] (from TGA curves)
ND CNC	132 (±1)	174 (±4)	8.2 (±1)	196 (±1)	307 (±4)	36 (±3)
FD CNC	132 (±1)	166 (±5)	4.5 (±1)	186 (±1)	287 (±7)	29 (±2)

comparison of T_d, T_{max}, and weight loss at T_{max} of FD CNC and ND CNC films.

From the DSC thermograms (**Figure 8**), initially steady endothermic heat flows up to around 80 and 90 °C were observed for the ND and FD CNC films, respectively, which corresponds to the phenomenon of physical dehydration and water vaporization.[54] No glass transition peak was noticed for these films within the temperature region investigated due to their highly crystalline nature.[4,55] The onset of exothermic peaks for both films at around 150 °C (with peak maxima at 172 °C) suggests the compaction of amorphous regions (which comprise ≈11% of this sulfuric acid hydrolyzed CNC, evaluated via XRD and discussed in the later section) of cellulose due to removal of residual bound water which was not removed during the film drying process.[56] Similar peaks were also identified at 174 and 166 °C for ND and FD CNC films, respectively in their DTG curves (see Figure 7b). At 192 °C, the ND CNC film showed the onset of exothermic heat flow due to the initiation of a major combustion reaction in the crystalline region, which was also observed at 196 °C from the DTG curves. The onset of sharp endothermic heat flow at 210 °C (with peak maximum at 238 °C and associated DTG peak at 240 °C, which was absent in ND CNC film) for FD CNC film might be due to the variation in the diffusion of heat of the various sized FD CNC flakes within the film, as mentioned earlier.

The XRD patterns of both ND CNC an FD CNC films demonstrated the characteristic major peak at 22.8°, with additional double peaks at 14.9° and 16.5° at room temperature (25 °C), as presented in **Figure 9**a,b, which is consistent with the diffraction
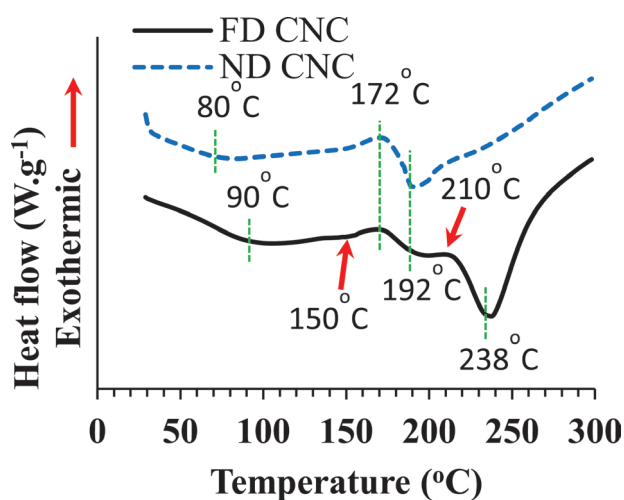
pattern of reference cellulose (ICDD patent PDF-2 database, File no. 00-050-2241).[57] However, with increasing temperature, the crystalline peak at 22.8° associated with the (200) crystal lattice plane of both FD and ND CNC films shifts to the lower diffraction angle. The peak intensity also decreases with increasing temperature (after normalizing the baseline, see inset in Figure 9a,b), suggesting the thermal degradation of the crystalline phase. The crystallinity index (CI) is found around 89% at 25 °C for both films (Figure 9c). A slight decrease in crystallinity to ≈84% is observed at 150 and 200 °C due to the initial thermal degradation, which correlates well with the TGA profile discussed above. A significant reduction in CI to ≈70% at 300 °C is due to the major combustion reaction involved at that temperature. At 300 °C, the FD CNC film showed comparatively lower CI (67%) compared to the ND CNC film (73%), which further points toward the more intense combustion reaction due to higher oxygen ingress within the flake-layered FD CNC film. At higher temperature (400 °C), both films completely lose their crystallinity as the XRD traces associated with the cellulose were absent due to combustion reaction and char formation. A similar effect has been reported for the microcrystalline cellulose by Yang et al.[58] showing the characteristic peaks of cellulose disappeared at 350 °C due to thermal decomposition reactions of the side groups.

The hydrophilic nature of CNC films can be represented by their low contact resistance to water. The measured contact angle of a water droplet placed on the FD CNC film revealed a rapid decrease from 30 ± 5° to 14 ± 4° within a minute before being fully absorbed onto the film surface (**Figure 10**a,b). This is expected due to the porous structure of the FD CNC film, as evidenced by the SEM image (see Figure 4a). In contrast, the water contact angle of ND CNC film showed a gradual decrease from 75 ± 4° to 18 ± 2° over 20 min due to the partial penetration of water into the film. It has been proposed that cellulose with a lower crystallinity swells more and faster.[59] However, in this study, despite the highly crystalline nature of the CNCs, there is evidence that sufficient pore space exists within the self-assembled ND CNC films for water sorption and film swelling to occur. The slightly rough surface (14 ± 4 nm, see Figure 4d) of this ND CNC film can allow water ingress into the film with time.

3. Conclusions

This work presents a comparative study between never-dried and freeze-dried CNCs on their morphological, microstructural, optical transparency, thermal, and crystallization properties. Upon freeze-drying, the needle-like ND CNCs yielded into flake-like geometries via aggregation, confirmed via TEM
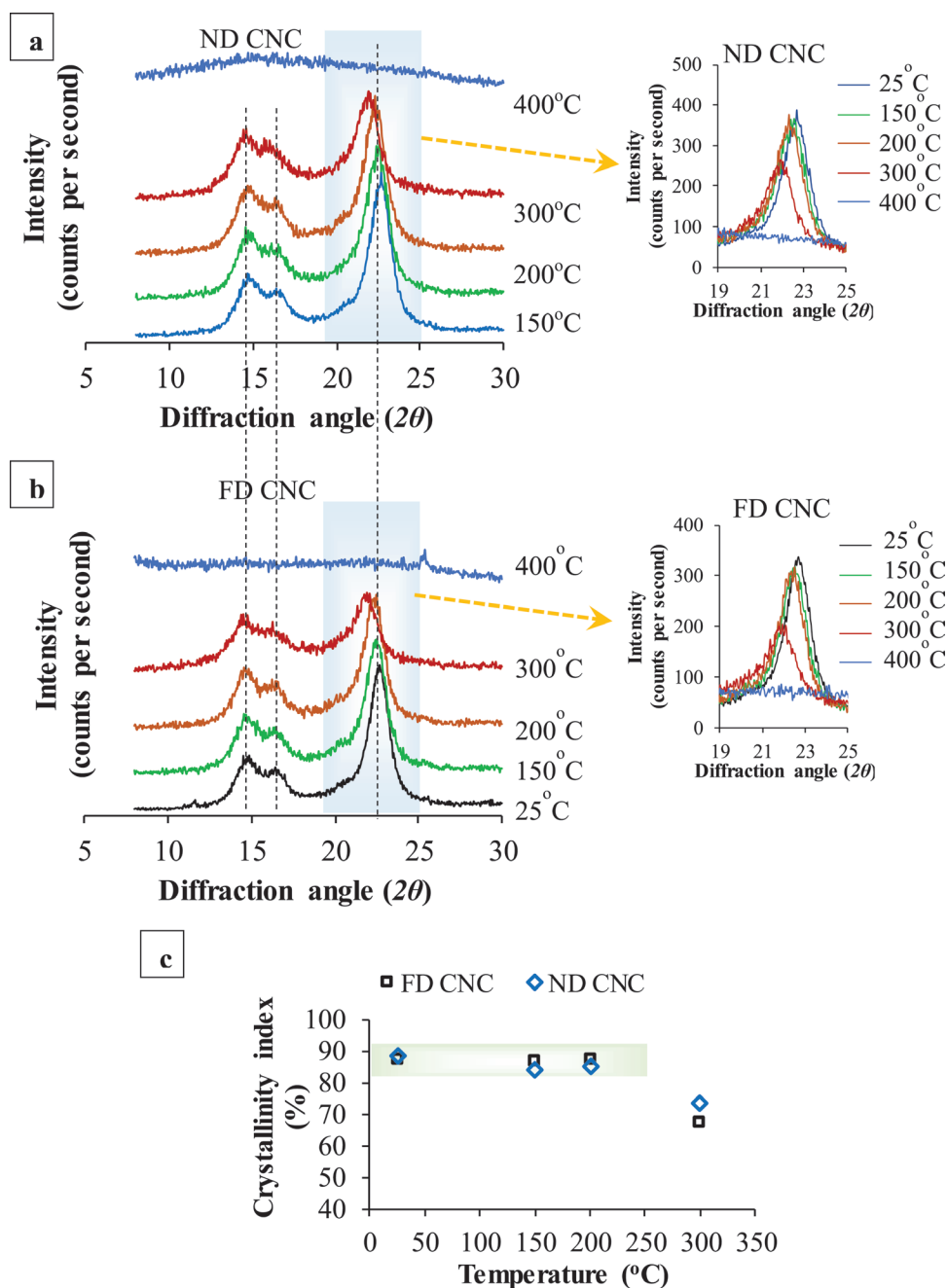

Figure 8. DSC thermographs of films produced from never-dried and freeze-dried CNCs.

ADVANCED
SCIENCE NEWS
www.advancedsciencenews.com

Macromolecular
Materials and Engineering
www.mme-journal.de

Figure 9. XRD Diffraction pattern of a) ND CNC and b) FD CNC films at various temperatures. c) crystallinity index (CI) of ND CNC and FD CNC films at various temperatures.

and SEM. In agreement with TEM, SAXS analysis on ND CNCs suspension and film also confirmed their needle-like structure with an average length of 140 nm (via fitting using a rigid elliptical cylinder model). The flake-like structure of the FD CNCs in aqueous suspension was unable to be fitted (via SAXS analysis) due to the sedimentation of the larger particles. However, the scattering pattern of FD CNC film was fitted using mass fractal model suggesting the internal film structure is fractal due to the compactness of the aggregated CNCs. Air-dried films produced from the FD CNCs displayed the formation of a white, opaque paper-like film due to their higher

surface roughness ($R_a = 134 \pm 20$ nm) created via random stacking of flakes compared to the transparent ND CNC film ($R_a = 14 \pm 4$ nm). No chemical change of the CNC was observed after the freeze-drying process, as confirmed via FTIR and EDX analyses; however, variation in their thermal degradation profile was observed. An intense major combustion reaction of FD CNC film compared to the ND CNC film was due to the higher amount of favorable oxygen ingress in the gaps created in between the FD CNC flakes. Therefore, a larger decrease in crystallinity of FD CNC film was also observed at a higher temperature (300 °C). Additionally, gaps created due to the random
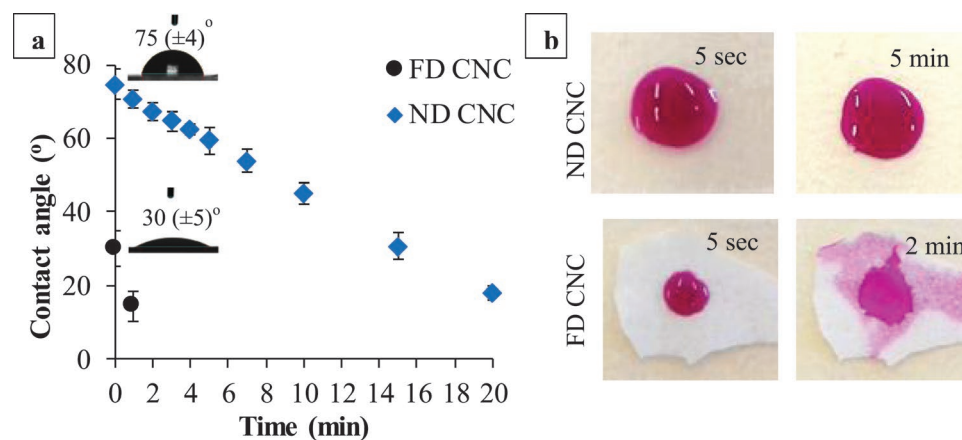
Figure 10. a) Change in the contact angle of a water droplet (10 μL) on ND CNC and FD CNC films over time (water droplet was fully absorbed on the FD CNC film surface within 2 min), b) photographs show the absorption of a dye solution (10 mg of Rhodamine B dye in 15 mL DI water) on the surface of ND and FD CNC films. Here, the dye solution was utilized for a visual effect only.

stacking of micron-sized FD CNC flakes within a film were shown to have a strong influence on increasing water absorption capacity.

In summary, films prepared from cotton hydrolyzed CNCs but from their never-dried and freeze-dried phases yielded different microscopic structure, optical, thermal, crystallization, and water absorption properties, though their chemical compositions were unaffected. These variable properties might be interesting to consider the use of these nanocrystals either alone or blending with a suitable matrix to extend their applications in diverse fields such as packaging, sustainable barrier films, drug delivery, coating, and separation sciences.

4. Experimental Section

Preparation of Cellulose Nanocrystals (CNCs): CNCs were produced by acid hydrolysis of cotton wool (Fisher Scientific, UK) using aqueous sulfuric acid (64 wt%) solution (Fisher Scientific, UK) for 45 min under continuous stirring, as described elsewhere.[28,60] The acid hydrolyzed CNCs suspension was centrifuged at 10 000 rpm at 10 °C for 20 min and redispersed using de-ionized (DI) water (three centrifugation cycles) followed by dialysis under DI water for 48 h to remove the residual acid. A Branson sonication probe (at 20% amplitude for 4 min using 4 s on and 1 s off pulsed mode) and then a filtration unit using a grade No. 2 fritted glass filter were utilized to disperse the CNC suspension. The obtained CNC suspension was treated overnight with Amberlite resin (Fisher Scientific, UK) to remove any non H_3O^+ cations. CNC dispersion was frozen in liquid nitrogen, before being freeze-dried to obtain the FD CNCs, as described elsewhere.[61]

Preparation of CNC Films: The ND CNC and FD CNC films were prepared via casting from their aqueous suspension followed by the air-drying process. ND CNC suspension was stable during the drying process, while sedimentation was seen in the FD CNC suspension after 10 min of homogenization (see Figure S1, Supporting Information). The homogenization process involved stirring the FD CNC suspensions (≈1.15 wt%) in de-ionized water using a magnetic stirrer for 2 h followed by utilizing an ultra-turrax (ULTRA-TURRAX, IKA T18 digital) for 15 min at 10 000 rpm. The suspensions were immediately poured into a polystyrene petri dish after homogenization and allowed to air dry for 48 h to obtain the films. Slow drying (air drying) was employed in a fume hood by placing the petri dish inside a cardboard box (≈300 mm of length × 300 mm of width × 150 mm of height at room temperature (≈25 to 27 °C) to avoid any crack formation in the films. Here, the box

was used to prevent direct contact of the airflow (toward ventilation area) with the evaporating suspension in the petri dish to minimize the wrinkle effect on the film surface. The films were further dried overnight in an oven at 50 °C before testing to eliminate traces of moisture.

Characterization—Electron Microscopic Analysis: The morphology of cotton wool, FD CNCs and films were examined using scanning electron microscopy (SEM – Philips XL30, FEI, USA) at an accelerating voltage of 10 kV and a working distance of 10 mm. Quantitative compositional analysis of the ND CNC and FD CNC films was carried out using an energy dispersive X-ray (EDX, INCA Oxford Instruments) detector. A sputtered platinum coating was employed to eliminate charging effects.

The size and shape of ND CNCs were characterized using transmission electron microscopy (TEM, JEOL, 2000FXII) at an accelerating voltage of 80 kV. The ND CNC sample loaded on a Cu-grid (mesh size 300) was negatively stained with uranyl acetate (2 wt%, Sigma-Aldrich, UK) to enhance the image contrast.

Characterization—Small Angle X-Ray Scattering (SAXS) Analysis: SAXS measurements on the ND and FD CNC suspensions with various concentrations (0.05, 0.1, 0.5, and 1.0 wt%) in DI water were conducted at Diamond Light Source (Didcot, Oxfordshire, UK), on the I22 beamline (X-ray wavelength of 1 Å and beam energy of E = 12.4 keV) equipped with a PILATUS P3-2M detector (Silicon hybrid pixel detector, DECTRIS). The FD CNC suspension was dispersed using a sonication probe (1 s on and 1 s off pulsed mode for a net time of 10 min at 30% amplitude, Ultrasonic Processor, FB-505) and then loaded in special glass capillary tubes (nominal diameter 1.5 mm, Capillary Tube Supplies Ltd, Bodmin, UK) and sealed. The scattering pattern from an empty capillary and a capillary containing DI water were also recorded for solvent background subtraction.[40] The probed q-range was 0.005–0.2 Å^{-1}. Data are provided in absolute scaling.

The intensity $I(q)$ can be written as follows

$$I(q) \propto P(q)S(q) \tag{1}$$

with $P(q)$ the form factor of the objects studied, giving information about their shape and $S(q)$ the structure factor associated with the interactions between the objects probed.

SAXS measurements of the film samples were performed on an Anton-Paar SAXSpoint 2.0 provided by the Material and Chemical Characterisation Facility (MC²)[62] equipped with a copper source (Cu K-α, λ = 1.542 Å) and a 2D EIGER R series Hybrid Photon Counting (HPC) detector. The distance between the film sample holder (containing ND and FD CNC films) and the detector was 556.9 mm and the data were collected at 25 °C in one frame, with 900 s exposure covering the q range of about 0.07–1.8 Å^{-1}. SASView software (version 4.1.2) was used to fit the SAXS data using a rigid elliptical cylindrical and mass fractal models.[40]

Characterization—Surface Charge: A dilute CNC suspension (0.1 wt% in DI water) was used to measure the ζ-potential utilizing a Malvern Zeta-sizer

Nano ZSP (Malvern, UK). Samples were placed in a folded capillary electrode cell and equilibrated at 25 °C for 120 s prior to testing. The data were taken from an average of 5 measurements from 100 scans each.

Characterization—Atomic Force Microscopy (AFM) Analysis: The ND CNC and FD CNC films were fixed onto microscope glass slides using double-sided polyimide Kapton tape to maintain them flat. AFM micrographs and roughness (Arithmetic Mean Average) measurements of the samples were performed in tapping mode utilizing a Bruker Dimension Icon equipped with an AFM tip (model RTESPA-150 0.01–0.025 Ohm cm Antinomy (n) doped Si). The tip on the cantilever interacts with materials surface to provide morphological information. The tip moved over the sample surface, producing a 3D image of the surface morphology. All measurements were carried out over a scan area of 5 µm^2. The obtained micrographs were analyzed utilizing Nanoscope analysis software (Version 1.5), and roughness analysis (Ra) was determined from at least three scans.

Characterization—Light Transmittance: Light transparency properties of the ND CNC and FD CNC films were determined by measuring the light transmittance using a UV–vis spectrometer (PerkinElmer, Lambda-25) over the wavelength range of 200 to 800 nm.

Characterization—Fourier Transform Infrared Spectroscopy (FTIR): The principal chemical groups present in ND CNC and FD CNC films were identified using an FTIR spectroscopy (PerkinElmer, Spectrum 100, USA) equipped with a standard attenuated total reflectance (ATR) cell. The films were scanned in transmittance mode over the wavenumber range from 4000 to 650 cm^{-1}, and the obtained spectra were analyzed using OPUS software (version 5.5).

Characterization—Thermogravimetric Analysis (TGA): TGA was performed on a TGA Q500 (TA Instruments) from 25 to 500 °C with a heating rate of 10 °C min^{-1} under airflow. TA Universal Analysis 2000 software was used to calculate the weight loss (%) and the derivative weight loss of the films with temperature from the TGA scans.

Characterization—Differential Scanning Calorimetry (DSC): DSC analysis was conducted utilizing a DSC Q20 (V24.10 Build 122) from TA Instruments over a temperature range from 25 to 300 °C at a heating rate of 10 °C min^{-1} under argon gas flow (18 mL min^{-1}). A blank pan measurement was conducted for background, and at least two tests were done for each film ($\approx$5 mg) to ensure repeatability.

Characterization—X-Ray Diffraction (XRD) Analysis: X-ray diffraction patterns for ND CNC and FD CNC films at different temperatures (25, 150, 200, 300, and 400 °C) were determined using a Bruker D8 Advanced diffractometer equipped with a Cu-Kα radiation source (λ = 0.15 406 nm) at 35 mA and 40 kV. The film samples were heated from room temperature to 400 °C at a heating rate of 10 °C min^{-1} and were equilibrated at a specific temperature for 1 min prior to scan from 7° to 30° diffraction angle (2θ) with a step size of 0.04° and 2 s time interval.

The crystallinity index (CI%) of the films was calculated according to the following equation[63,64]

$$CI[\%] = \frac{I_{(Crys+am)} - I_{(am)}}{I_{(Crys+am)}} \times 100 \qquad (2)$$

Where $I_{(Cry+am)}$ denotes the most intense peak attributed to the combined crystalline (Crys) and amorphous (am) parts of cellulose (peak intensity at 2θ = 22.8°), whereas $I_{(am)}$ represents the amorphous portion of cellulose (peak intensity usually appearing at 2θ = 18°).

Characterization—Water Contact Angle: The water contact angles of the films were measured using a drop tensiometer (OCA 20, Dataphysics Co., Germany) at ambient temperature. A 10 µL of DI water drop was deposited via a microsyringe on the CNC film surface, and the contact angles were measured at different time points. The reported contact angle value was taken from an average of 5 measurements.

Supporting Information

Supporting Information is available from the Wiley Online Library or from the author.

Conflict of Interest

The authors declare no conflict of interest.

[1] D. Klemm, F. Kramer, S. Moritz, T. Lindström, M. Ankerfors, D. Gray, A. Dorris, *Angew. Chem., Int. Ed.* **2011**, *50*, 5438.

[2] S. J. Eichhorn, A. Dufresne, M. Aranguren, N. E. Marcovich, J. R. Capadona, S. J. Rowan, C. Weder, W. Thielemans, M. Roman, S. Renneckar, W. Gindl, S. Veigel, J. Keckes, H. Yano, K. Abe, M. Nogi, A. N. Nakagaito, A. Mangalam, J. Simonsen, A. S. Benight, A. Bismarck, L. A. Berglund, T. Peijs, *J. Mater. Sci.* **2010**, *45*, 1.

[3] D. Trache, M. H. Hussin, M. K. M. Haafiz, V. K. Thakur, *Nanoscale* **2017**, *9*, 1763.

[4] B. L. Pelegrini, F. Ré, M. M. De Oliveira, T. Fernandes, J. H. Oliveira, A. G. Oliveira Junior, E. M. Girotto, C. V. Nakamura, A. R. Sampaio, A. Valim, M. M. Souza Lima, *Macromol. Mater. Eng.* **2019**, *304*, 1900092.

[5] K. A. Mahmoud, J. A. Mena, K. B. Male, S. Hrapovic, A. Kamen, J. H. T. Luong, *ACS Appl. Mater. Interfaces* **2010**, *2*, 2924.

[6] C. Endes, O. Schmid, C. Kinnear, S. Mueller, S. Camarero-Espinosa, D. Vanhecke, E. J. Foster, A. Petri-Fink, B. Rothen-Rutishauser, C. Weder, M. J.d Clift, *Part. Fibre Toxicol.* **2014**, *11*, 40.

[7] R. M. A. Domingues, M. Silva, P. Gershovich, S. Betta, P. Babo, S. G. Caridade, J. F. Mano, A. Motta, R. L. Reis, M. E. Gomes, *Bioconjugate Chem.* **2015**, *26*, 1571.

[8] E. Lam, K. B. Male, J. H. Chong, A. C. W. Leung, J. H. T. Luong, *Trends Biotechnol.* **2012**, *30*, 283.

[9] A. Barbosa, E. Robles, J. Ribeiro, R. Lund, N. Carreño, J. Labidi, *Materials* **2016**, *9*, 1002.

[10] R. J. Moon, A. Martini, J. Nairn, J. Simonsen, J. Youngblood, *Chem. Soc. Rev.* **2011**, *40*, 3941.

[11] Y. Habibi, L. A. Lucia, O. J. Rojas, *Chem. Rev.* **2010**, *110*, 3479.

[12] M. T. Islam, M. M. Alam, A. Patrucco, A. Montarsolo, M. Zoccola, *AATCC J. Res.* **2014**, *1*, 17.

[13] J. Araki, M. Wada, S. Kuga, T. Okano, *Colloids Surf. A* **1998**, *142*, 75.

[14] Y. Zhao, C. Moser, M. E. Lindström, G. Henriksson, J. Li, *ACS Appl. Mater. Interfaces* **2017**, *9*, 13508.

[15] S. Ummartyotin, H. Manuspiya, *Renewable Sustainable Energy Rev.* **2015**, *41*, 402.

[16] A. Isogai, T. Saito, H. Fukuzumi, *Nanoscale* **2011**, *3*, 71.

[17] C. Moser, M. E. Lindström, G. Henriksson, *BioResources* **2015**, *10*, 2360.

[18] K. Fleming, D. Gray, S. Prasannan, S. Matthews, *J. Am. Chem. Soc.* **2000**, *122*, 5224.

[19] S. Dong, M. J. Bortner, M. Roman, *Ind. Crops Prod.* **2016**, *93*, 76.

[20] M. N. Anglès, A. Dufresne, *Macromolecules* **2000**, *33*, 8344.

[21] G. Siqueira, J. Bras, A. Dufresne, *Biomacromolecules* **2009**, *10*, 425.

[22] Y. Habibi, A.-L. Goffin, N. Schiltz, E. Duquesne, P. Dubois, A. Dufresne, *J. Mater. Chem.* **2008**, *18*, 5002.

[23] M. Shahrousvand, F. A. Tabar, E. Shahrousvand, A. Babaei, M. M. Hasani-Sadrabadi, G. M. M. Sadeghi, H. Jafari, A. Salimi, *Carbohydr. Polym.* **2017**, *175*, 293.

[24] A. Dufresne, *Mater. Today* **2013**, *16*, 220.

[25] A. B. Reising, R. J. Moon, J. P. Youngblood, *J. Sci. Technol. For. Prod. Processes* **2012**, *2*, 32.

[26] I. A. Rahman, P. Vejayakumaran, C. S. Sipaut, J. Ismail, C. K. Chee, *Ceram. Int.* **2008**, *34*, 2059.

[27] X. M. Dong, D. G. Gray, *Langmuir* **1997**, *13*, 2404.

[28] K. M. Z. Hossain, I. Ahmed, A. J. Parsons, C. A. Scotchford, G. S. Walker, W. Thielemans, C. D. Rudd, *J. Mater. Sci.* **2012**, *47*, 2675.

[29] N. Lavoine, L. Bergström, *J. Mater. Chem. A* **2017**, *5*, 16105.

[30] N. Lavoine, I. Desloges, A. Dufresne, J. Bras, *Carbohydr. Polym.* **2012**, *90*, 735.

[31] J. S. Taurozzi, V. A. Hackley, M. R. Wiesner, *Nanotoxicology* **2011**, *5*, 711.

[32] V. Khoshkava, M. R. Kamal, *Powder Technol.* **2014**, *261*, 288.

[33] J. George, S. S N, *Nanotechnol., Sci. Appl.* **2015**, *8*, 45.

[34] J. Han, C. Zhou, Y. Wu, F. Liu, Q. Wu, *Biomacromolecules* **2013**, *14*, 1529.

[35] A. J. Svagan, M.y A. S. A. Samir, L. A. Berglund, *Adv. Mater.* **2008**, *20*, 1263.

[36] J. Lee, Y. Deng, *Soft Matter* **2011**, *7*, 6034.

[37] T. Phan-Xuan, A. Thuresson, M. Skepö, A. Labrador, R. Bordes, A. Matic, *Cellulose* **2016**, *23*, 3653.

[38] Y. Liu, D. Stoeckel, K. Gordeyeva, M. Agthe, C. Schütz, A. B. Fall, L. Bergström, *ACS Macro Lett.* **2018**, *7*, 172.

[39] S. Deville, *Science* **2006**, *311*, 515.

[40] J. Schmitt, V. Calabrese, M. A. Da Silva, S. Lindhoud, V. Alfredsson, J. L. Scott, K. J. Edler, *Phys. Chem. Chem. Phys.* **2018**, *20*, 16012.

[41] C. M. Sorensen, *Aerosol Sci. Technol.* **2001**, *35*, 648.

[42] S. Beck, J. Bouchard, G. Chauve, R. Berry, *Cellulose* **2013**, *20*, 1401.

[43] M. Nogi, S. Iwamoto, A. N. Nakagaito, H. Yano, *Adv. Mater.* **2009**, *21*, 1595.

[44] R. Rusli, S. J. Eichhorn, *Appl. Phys. Lett.* **2008**, *93*, 033111.

[45] Q. Li, J. Zhou, L. Zhang, *J. Polym. Sci., Part B: Polym. Phys.* **2009**, *47*, 1069.

[46] J. Xiong, Q. Li, Z. Shi, J. Ye, *Food Res. Int.* **2017**, *100*, 858.

[47] Z. Man, N. Muhammad, A. Sarwono, M. A. Bustam, M. Vignesh Kumar, S. Rafiq, *J. Polym. Environ.* **2011**, *19*, 726.

[48] A. Kumar, Y. Singh Negi, V. Choudhary, N. Kant Bhardwaj, *J. Mater. Phys. Chem.* **2020**, *2*, 1.

[49] I. C. Mcneill, S. Ahmed, S. Rendall, *Polym. Degrad. Stab.* **1998**, *62*, 85.

[50] O. V. Khutoryanskaya, V. V. Khutoryanskiy, R. A. Pethrick, *Macromol. Chem. Phys.* **2005**, *206*, 1497.

[51] K. M. Zakir Hossain, L. Jasmani, I. Ahmed, A. J. Parsons, C. A. Scotchford, W. Thielemans, C. D. Rudd, *Soft Matter* **2012**, *8*, 12099.

[52] W.-P. Pan, G. N. Richards, *J. Anal. Appl. Pyrolysis* **1989**, *16*, 117.

[53] S. Julien, E. Chornet, P. K. Tiwari, R. P. Overend, *J. Anal. Appl. Pyrolysis* **1991**, *19*, 81.

[54] J. Scheirs, G. Camino, W. Tumiatti, *Eur. Polym. J.* **2001**, *37*, 933.

[55] Y. H. Roos, *Annu. Rev. Food Sci. Technol.* **2010**, *1*, 469.

[56] T. V. Smotrina, A. T. Kynin, S. F. Grebennikov, *Russ. J. Appl. Chem.* **2004**, *77*, 480.

[57] M. M. Abou-Sekkina, M. A. Sakran, A. A. Saafan, *Ind. Eng. Chem. Prod. Res. Dev.* **1986**, *25*, 676.

[58] J.-W. Yang, J. S. Won, D. Y. Jin, J. E. Lee, W. H. Park, S. G. Lee, *Green Compos. Mater.* **2015**, *2015*, 1.

[59] M. Ghasemi, P. Alexandridis, M. Tsianou, *Biomacromolecules* **2018**, *19*, 640.

[60] K. M. Z. Hossain, M. S. Hasan, D. Boyd, C. D. Rudd, I. Ahmed, W. Thielemans, *Biomacromolecules* **2014**, *15*, 1498.

[61] M. Labet, W. Thielemans, *Cellulose* **2011**, *18*, 607.

[62] "Material and Chemical Characterisation Facility (MC²)", The University of Bath, p. 2019.

[63] L. Segal, J. J. Creely, A. E. Martin, C. M. Conrad, *Text. Res. J.* **1959**, *29*, 786.

[64] P. J. Weimer, J. M. Hackney, A. D. French, *Biotechnol. Bioeng.* **1995**, *48*, 169.